An Integrated Decision, Control and Fault Detection Scheme for Cooperating Unmanned Vehicle Formations

N. Léchevin, C.A. Rabbath, M. Shanmugavel, A. Tsourdos and B.A. White

Abstract— We propose a hierarchical and decentralized scheme for integrated decision, control and fault detection in cooperating unmanned aerial systems flying in formations and operating in adversarial environments. To handle, in a cooperative fashion, events that may adversely affect the outcome of a multivehicle mission, events such as actuator faults, body damage, network interruption/delays, and vehicle loss, we present a decision-control system whose architecture comprises three main components: formation control and trajectory generation, abrupt and nonabrupt fault detection, and decision-making relying on optimization under uncertainty. The scheme seeks to provide the most effective team adaptation to contingencies despite partially known environments and limited available information. The integrated decision, control and fault detection scheme is demonstrated numerically by means of high-fidelity, nonlinear 6-DOF simulations of multiple formation flying airships. For a rendezvous mission, the paper shows that concurrent nonabrupt and abrupt type faults can be detected and effectively compensated for both at the formation control and at the decision-making levels, despite network mishaps, which represents a novelty in itself.

I. INTRODUCTION

It is envisaged that future unmanned and joint manned-unmanned air missions will include cooperative sensor networks for search and rescue, surveillance and monitoring over civilian populated zones, and cooperating networked UAVs and weapons for engagements of mobile targets. However, despite decision, guidance and control, fault-tolerant control (FTC), and fault detection, isolation and recovery (FDIR) software embedded onboard the air vehicles and on networked control stations, overall mission performance may still be degraded after the occurrence of harmful events. Under severe body damage or actuator faults, post-fault system dynamics may differ considerably from pre-fault dynamics so that the control authority may be significantly reduced. In such occasions, the faulty vehicle is not capable of performing its assigned task with the expected level of efficiency. Furthermore, for slowly developing onboard malfunctions, or nonabrupt faults, individual vehicle FDIR and FTC typically provide limited recovery. There is therefore a need to develop and to demonstrate, schemes that provide highly efficient and reliable cooperation of air vehicles, and that adapt to the occurrence of a variety of events.

Only few results offering a limited capability of event monitoring and team adaptation are currently available.

N. Léchevin is with Numerica Technologies. C.A. Rabbath is with Defence R&D Canada Valcartier (nicolas.lechevin.numerica, camille-alain.rabbath@drdc-rddc.gc.ca). M. Shanmugavel, A. Tsourdos and B.A. White are with Cranfield University (a.tsourdos@cranfield.ac.uk).

Mission-level functional reliability is tackled in [1] through centralized planning and health management. Reconfiguration strategies for UAV formations facing network faults were proposed in [2], based on graph theory and a modified Dijkstra algorithm, whereas [3] relied on interacting-multiple-model FDI for such faults. A decentralized, cooperative fault detection and control adaptation scheme for formation flying air vehicles faced with intermittent network loss concurrent with a single actuator fault was proposed in [4]. This novel technique is effective only for abrupt-type actuator faults, short-duration network unavailability, and specific formations. A networked decision and information system was proposed in [5] for rendezvous type combat missions in spite of conflicting objectives of opposing teams, stochastic dynamics, and imperfect information on the adversary. Yet, there remains to evaluate the performance of the decision system under a realistic, real-time framework.

This paper proposes a hierarchical and decentralized scheme for integrated decision, control and fault detection in cooperative UAVs flying in formations and engaged in an adversarial environment. The objective is to achieve mission success despite the occurrence of events that may adversely affect the outcome. In such context, cooperative monitoring and then adaptation to harmful events is required. To do so, we present a new decision-control system whose architecture comprises three main components: formation control and trajectory generation, nonabrupt and abrupt fault detection, and decision-making relying on optimization under uncertainty. The integrated decision, control and fault detection scheme is demonstrated by means of high-fidelity, nonlinear 6-DOF simulations of formation flying airships. For rendezvous missions, it is shown that concurrent nonabrupt and abrupt type faults, incomplete information, and vehicle loss can be effectively compensated for both at the formation control and at the decision-making levels.

II. INTEGRATED DECISION, CONTROL AND FAULT DETECTION

Figure 1 presents the architecture of the proposed integrated decision, control and fault detection (I-DCFD). It can be seen that the various functions are performed separately, although the systems exchange information either via the network or from the available sensors. I-DCFD is available in each formation, with computing carried out either in each vehicle of a formation. I-DCFD is composed of (i) Component-Level (CL) FDIR, which deals with actuator and fault failures, (ii) Team-Level (TL) FDIR, which preserves formation flight performance for faults or failures that cannot be compensated for by the CL FDIR, and (iii) decision-making in closed loop with the information management. The decision process aims at maximizing the weapon effect of p formations over a set of

targets, while accounting for the loss of vehicles [5]. TL FDIR is composed of Decentralized Abrupt Fault Detection (DAFD) and Decentralized Nonabrupt Fault Detection (DNFD) systems. In the sequel, CL FDIR is not discussed. Details can be found in [7], [8].
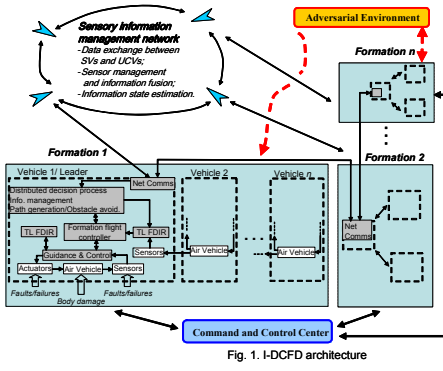
Fig. 1. I-DCFD architecture

A. Formation Control & Trajectory Generation

1) Formation Control

A group of p leader-to-follower formations is considered each of which is composed of n vehicles. The leader tracks a reference trajectory. The leader is labeled as node 1, whereas the followers are nodes 2 to n. Associate to each node i the set $\mathcal{N}_i$, which includes the ith node and all the neighboring vehicles j that are sensed by i. $\mathcal{N}_i$ is endowed with a neighboring unidirectional relation, where sensory data (position and velocity of j) flows from $j \in \mathcal{N}_i$ to i; i.e., i measures its distance relative to j. The formation geometry is characterized by angle λ_{ij}^* and relative distances ρ_{ij}^*, assumed time-invariant. Such information is transmitted from one node to another according to $G_{FFC} = (S, E_{FFC})$, where $S = \{1, ..., n\}$ and $E_{FFC} = \{(i, j); i, j \in S, j \in \mathcal{N}_i\}$. G_{FFC} represents sensory data flow for formation flight control purpose. Vehicle dynamics is

$$M\ddot{x}_i = \sum_j F_{ji}\sin(\gamma_i) - C_x\dot{x}_i, \quad M\ddot{y}_i = \sum_j F_{ji}\sin(\phi_i) - C_x\dot{y}_i$$

$$M\ddot{z}_i = -\sum_j F_{ji}\cos(\gamma_i)\cos(\phi_i) - F_B + F_g - C_z\dot{z}_i$$

$$J_\theta\ddot{\theta}_i = (F_{1i}l_1 - F_{2i}l_2 + F_{3i}l_3 - F_{4i}l_4)\sin(\rho_i) - C_\theta\dot{\theta}_i \quad (1)$$

$$J_\gamma\ddot{\gamma}_i = F_{1i}l_1 - F_{3i}l_3 - F_Bl_B\sin(\gamma_i) - C_\gamma\dot{\gamma}_i$$

$$J_\phi\ddot{\phi}_i = -F_{2i}l_2 + F_{4i}l_4 - F_Bl_B\sin(\phi_i) - C_\phi\dot{\phi}_i,$$

$x_i' = x_i + w_x$, $y_i' = y_i + w_y$, $\theta_i' = \theta_i + w_\theta$, $\gamma_i' = \gamma_i + w_\gamma$, $\phi_i' = \phi_i + w_\phi$

where x_i, y_i, z_i are vehicle translations w.r.t. inertial frame I_{xyz}; θ, ϕ, and γ are vehicle rotations; M is the mass of each vehicle; J_ϕ, J_γ and J_θ are the moments of inertia about the x, y, and z axes; F_g is the force due to gravity; F_B is the buoyant force; F_{ji} is the force magnitude of the jth motor, $j \in \{1,2,3,4\}$; l_j are the perpendicular distances between motors j and center of mass; C_X is the drag coefficient in the direction $X \in \{x, y, z, \theta, \phi, \gamma\}$ which serves as a damping term for the motion in that direction; and ρ is the angular offset from the vertical axis of the motor thrust vectors. Measurement of the state is corrupted by Gaussian noise $w_X \sim \mathcal{N}(0, \sigma_{w_X})$. The flight control and guidance laws consist of a set of PID controllers [4]. The outer-loop control generates pitch and roll commands (u_x, u_y) to move the vehicle in the (x, y) space. The outer-loop decentralized control of the leader of the formation, which is characterized by Cartesian state (x_o, y_o, z_o), is $u_{xo} = k_p(x^* - x_o') - k_d\dot{x}_o'$, $u_{yo} = k_p(y^* - y_o') - k_d\dot{y}_o'$, where x^* and y^* are reference trajectories to be followed by the leader, as obtained from the trajectory generator discussed in the following subsection [6]. x^* and y^*

are also available to vehicles $i \in \mathcal{N}_1$. Guidance for the follower $i \in S \setminus \{0\}$ with state (x_i, y_i, z_i) is given as [6]

$$[u_{xi}\ u_{yi}]^T = h_i(\sum_{j \in \mathcal{N}_i} k_i[x_j' - x_i' - x_{ij}^* \mid y_j' - y_i' - y_{ij}^*]^T),$$

$$[x_{ij}^*\ y_{ij}^*]^T = \rho_{ij}^*[\cos(\lambda_{ij}^* + \psi_i)\sin(\lambda_{ij}^* + \psi_i)]^T, \quad (2)$$

where ψ_i is the heading angle of i. h_i is a strict positive real operator whose stabilizability property is derived in [6].

2) Trajectory Generation

Trajectory generation is carried out for the formation leaders, in the form of x^* and y^* commands. Trajectory generation involves producing flyable trajectories, i.e., those satisfying inherent kinematic limits and induced dynamic limits of the vehicles. Mathematically, the kinematic variables are proportional to the intrinsic variables of a curve; e.g., the lateral acceleration is proportional to the curvature of the curve. We use Pythagorean Hodograph (PH) curve $r(t)$ given as $r(t) = (x(t), y(t))$, $(dx(t)/dt)^2 + (dy(t)/dt)^2 = \sigma(t)^2$, where $\sigma(t)$ is a complex polynomial $\sigma(t) = u(t) + iv(t)$, such that $\text{Re}(\sigma(t)^2) = (dx(t)/dt)^2$, $\text{Im}(\sigma(t)^2) = (dy(t)/dt)^2$, $\text{Re}(\sigma(t)^2) = u(t)^2 - v(t)^2$, and $\text{Im}(\sigma(t)^2) = 2u(t)v(t)$. PH curve is known for its curvature and torsion being rational and exact calculations of the trajectory length, exempt of numerical approximations. With I-DCFD, waypoints are connected by means of a PH curve and threat/collision avoidance is obtained by creating an intermediate waypoint. Consider trajectory $r(t)$, which is generated for a set of poses/waypoints. The threat avoidance algorithm calls the trajectory generator to re-plan the nominal PH trajectory, obtained prior to occurrence of a threat, by providing a new waypoint/pose in the event of an

Fig. 2: Nominal (blue) and re-planned (green) PH trajectories

intersection with the threat. The schematic is given in Fig. 2, where the red patch is a threat. WP1 and WP2 are waypoints. $r(t)$ is the nominal PH trajectory. The intermediate waypoint M is selected based on the location of the centre of threat C, being either to the left or to the right of the line connecting the intersection points X_1 and X_2. If the center C is to the left of the line X_1-X_2, M is selected to the right of the threat region. The waypoints are on the safety circle for the UAV; e.g., M and N on the safety circle are generated by intersecting the normal to the line segment X_1-X_2 with the safety circle. The new path generated with M is composed of PH curves $r_1(t)$ and $r_2(t)$.

B. Decentralized Nonabrupt and Abrupt Fault Detection

Monitoring neighboring vehicles enables cooperative fault detection, when faults cannot be compensated for at a satisfactory level by the CL FDIR. A problematic situation arises when communications are lost intermittently and possibly concurrently with the occurrence of component faults. The state of the formations cannot be published across the network at the time of faults, and hence sensory data onboard the UAVs become the redundant information that can be used by I-DCFD.

1) Modeling of Faults

With reference to (1), the signal of interest is denoted as F_i

(t). Such signal can represent either actuator output force $F_i(t)$ or an exogenous force such as buoyancy F_B. Let t_f denote the time at which a CL fault occurs. Faults can be either abrupt or nonabrupt. $F_i(t)$ can be formally expressed, for $i \in S$, as $F_i(t) = K_i(t_f, t, F_{in}(t))$ where $F_{in}(t)$ denotes the nominal signal exempt from a fault. K_i is the identity function, i.e., $F_i(t) = F_{in}(t)$, when $t < t_f$ and a polynomial function of F_{in} when $t \geq t_f$. K_i is typically nondifferentiable at t_f. $F_i(t)$ can be expressed as

$$F_i(t) = F_{in}(t) - F_{in}(t) + K_i(t_f, t, F_{in}(t)) \qquad (3)$$
$$= F_{in}(t) - \delta_i(t_f).$$

Faults whose dynamics are significantly faster than those of the nominal vehicle are labeled as abrupt [9]. Abrupt changes are modeled by means of discontinuous functions $\delta_i(t_f)$, where $\delta_i(t_f^+) - \delta_i(t_f^-)$ is sufficiently large to yield fast time-drifting response of the closed-loop dynamics.

Performance degradation in aircraft flight can be generally attributed to (F1) actuator fault, and (F2) body damage.
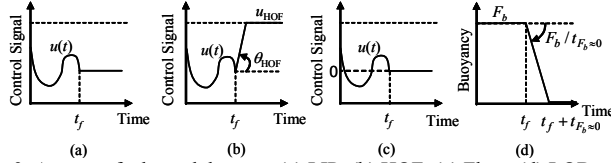
Fig. 3. Actuator faults and damage. (a) LIP; (b) HOF; (c) Float; (d) LOB.

They include Lock In Place (LIP), Hard-Over Failure (HOF), float and loss of effectiveness [9], as shown in Fig. 3. Body damage of the ALTAV may result in a loss of buoyancy (LOB), which can be either sudden ($t_{F_b \approx 0} \approx 0$) or gradual ($t_{F_b \approx 0} \gg 1$). Two types of abrupt faults can occur with the ALTAV: HOF with $1 - u(t_f)/u_{HOF} \approx 1$ and $\theta_{HOF} \approx \pi/2$, and sudden loss of buoyancy. The CHM scheme known as DAFD [5] is able to detect the two aforementioned abrupt faults. Particular ALTAV actuator faults of types LIP ($\delta_i(y) = u(t_f)$, $t \geq t_f$) and float ($\delta_i(y) = 0$ when $u(t_f) = 0$, $t \geq t_f$), as well as gradual HOF and LOF constitute the class of nonabrupt faults that cannot be distinguished from noise in the detector's residues by DAFD. Such facts motivate the design of a complementary fault detector, the DNFD.

2) Decentralized Abrupt Fault Detector

The DAFD is developed and tuned from a simplified state-space [4]. To represent the time-varying flight envelope and to account for possible bounded parametric uncertainties, the following linearly parameterized system is proposed

$$\dot{q}_i = A_i(\alpha_i) q_i + B_i(\alpha_i) \underbrace{\begin{bmatrix} h_i \sum_{j \in N_i} k_i(x_j - x_{ij}^*) \\ h_i \sum_{j \in N_i} k_i(y_j - y_{ij}^*) \\ z_t \end{bmatrix}}_{v_{i1} - v_{i2}}, \begin{bmatrix} v \\ y_i \\ z_i \end{bmatrix} = \begin{bmatrix} q_{i1} \\ q_{i3} \\ q_{i6} \end{bmatrix} \qquad (4)$$

where $[x_{ij}^* \; y_{ij}^*]^T = \rho_{ij}^* [\cos(\lambda_{ij}^* + \psi_i) \; \sin(\lambda_{ij}^* + \psi_i)]^T$, $q_i = [\ q_{i1} \ q_{i2} \ q_{i3} \ q_{i4} \ q_{i5} \ q_{i6}]^T$; x_i, y_i, and z_i are the vehicle translations; ψ_i is the heading angle of vehicle i; z_t is the prescribed altitude of the formation, known prior to mission. α_i is assumed to evolve within $\Gamma_i = \{(\alpha_{i1,\dots,} \alpha_{is}) | \sum_{j=1}^s \alpha_{ij} = 1, \; \alpha_{ij} \geq 0\}$. The state space is linear in α; i.e., $[A_i(\alpha) | B_i(\alpha)] = \sum_{j=1}^s \alpha_{ij} [A_{ij} | B_{ij}]$. $A_i(\alpha)$ (resp., $B_i(\alpha)$) can be decomposed as the sum of a nominal matrix $A_i^* = A_i(\alpha^*)$ (resp., $B_i^* = B_i(\alpha^*)$) and a deviation matrix $\tilde{A}_i(\alpha)$ (resp., $\tilde{B}_i(\alpha)$) that evolves in the same polytope as that

of $A_i(\alpha)$ (resp., $B_i(\alpha)$); i.e., $\tilde{A}_i(\alpha) = \sum_{j=1}^s \alpha_{ij} \tilde{A}_{ij}$ and $\tilde{B}_i(\alpha) = \sum_{j=1}^s \alpha_{ij} \tilde{B}_{ij}$. The model in (4) for $i \in N_k$, which is used by vehicle k to detect faults on neighboring vehicle i, is characterized by the unknown signal x_j, where j is in N_i, but not necessarily in N_k. Considering that x_{ij}^* in (4) is available to k, the proposed observer is

$$\dot{\hat{q}}_i = A_{F,i} \hat{q}_i + B_i^* \underbrace{\begin{bmatrix} h_i \sum_{j \in N_i} k_i(\hat{x}_j - x_{ij}^*) \\ h_i \sum_{j \in N_i} k_i(\hat{y}_j - y_{ij}^*) \\ z_t \end{bmatrix}}_{\hat{v}_{i1} - v_{i2}} + B_{F,i} C_i q_i, r_i = C_i q_i - C_{F,i} \hat{q}_i \qquad (5)$$

where

$$B_i^* \begin{bmatrix} h_i \sum_{j \in N_i} k_i \hat{x}_j & h_i \sum_{j \in N_i} k_i \hat{y}_j & 0 \end{bmatrix}^T = L^{-1} \left\{ \frac{B_i^* \hat{v}_{i1}(s)}{\tau_f s + 1} \right\} \\ = L^{-1} \left\{ \frac{\dot{\hat{q}}_i(s) - A_i^* \bar{q}_i(s) + B_i^* v_{i2}(s)}{\tau_f s + 1} \right\}, \qquad (6)$$

and

$$\bar{q}_i^T = [q_{i1} \ L^{-1}\{\frac{sx_i(s)}{\tau_d s + 1}\} \ q_{i3} \ L^{-1}\{\frac{sy_i(s)}{\tau_d s + 1}\} \ q_{i5} \ q_{i6}] \qquad (7)$$

where $\bar{q}_i$ is given in the time domain. Furthermore, $C_i = \begin{bmatrix} 1 & 0 & 0 & 0 & 0 & 0 \\ 0 & 0 & 1 & 0 & 0 & 0 \end{bmatrix}$, $v_{i2}^T = [-h_i \sum_{j \in N_i} k_i x_{ij}^* \ | -h_i \sum_{j \in N_i} k_i y_{ij}^* \ | z_t]$ and $q_i = \bar{q}_i + \breve{q}_i$. The error signal $\breve{q}_i$ is caused by the use of low-pass filtered derivatives in (7). τ_d and τ_f are time constants of low-pass filters used to obtain biproper transfer functions in (6) and (7) whenever a signal derivative is used. The observer in (5) is composed of $(A_{F,i}, B_{F,i}, C_{F,i})$, which are derived to minimize the impact of $\hat{x}_j$ and $\hat{y}_j$, and of coupling terms $\hat{x}_j - x_{ij}^*$ and $\hat{y}_j - y_{ij}^*$. The coupling terms represent the interaction of vehicle i with its neighbors $j \in N_i$. It is shown in [4] that the impact of disturbances due to modeling errors on the residue r_i in (5) is minimized in the L_2-gain sense if some LMI is satisfied.

3) Decentralized Nonabrupt Fault Detector

a) Networked Sensory Information and Coupling Effects

Let $j_i \in N_i$ and $k_{j,i} \in N_{j_i}$ be the neighbors of i and j_i, respectively.

Definition 1 (Faulty vehicle). Let $j_i^F \in N_i$ be the vehicle that is subject, at $t = t_f$, to a nonabrupt fault. The information sent from j_i^F is unreliable for the purpose of detection by i. Two or more nonabrupt faults cannot occur within $[t_f, t_f + \tau)$, where τ stands for the time interval needed to collect data and to perform hypothesis testing. T_s is the time step at which onboard sensor signals are updated.

Definition 2 (Data flow graph). The DNFD uses the data flow graph $G_{DNFD} = (S, E_{DNFD})$, with $S = \{1, ..., n\}$. E_{DNFD} is the set of directed edges (i, i), and $(i, k_{i,j})$, where $i, k_{i,j} \in V$, and $k_{j,i} \in N_{j_i}$. E_{DNFD} represents information flow relevant to DNFD; i.e., $k_{i,j}$ communicates its estimated heading angle $\hat{\psi}_{k_{j,i}}$ to i at a rate of $T_n = p T_s$, $p \in \mathbb{N}$, as shown in Fig. 4(a).
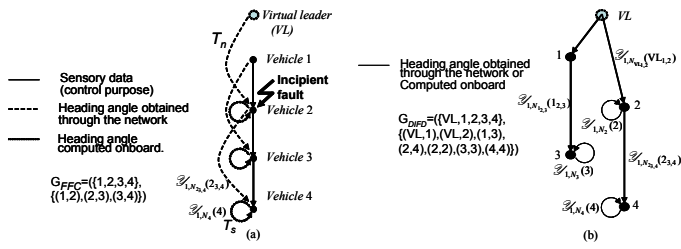
Fig.4. Formation flight control and DNFD. (a) Information network and sensory data flow; (b) Graph of information flow utilized by DNFD. Vehicles 2, 3, and 4 are able to detect faulty behavior of neighboring vehicles since their indegree is greater than or equal to 2.

The underlying principle of DNFD is to have any given vehicle i carrying out monitoring of vehicle j_i, which is assumed, by virtue of *Definition* 1, not to provide reliable data about its own behavior. i performs hypothesis testing on the comparison of the heading angle trajectory of $k_{j,i}$ with that of i to detect any faulty behavior. DNFD is thus based on the fact that each follower node of G_{DNFD} must have indegree greater than or equal to 2 to perform the comparison in the fault-no-fault hypothesis test. The motivation for the selection of the heading angle trajectory as a meaningful signal for the hypothesis test is explained in Fig. 5. Typical heading angle trajectory of $i \in S$ is shown in Fig. 5(a). The follower trajectory is similar to that of the leader, albeit with a time delay that results from dynamic couplings among adjacent vehicles in G_{FFC}, inherent to formation flight. A fault occurring at t_f in j_i^F entails either a new steady-state heading angle trajectory or a drifting trajectory, depicted in Fig 5(b) as curves (i) and (ii), respectively. The detector implemented onboard i at $t_k = kT_s$ consists in deriving a function $\mathscr{T}$ defined over $\mathscr{Y}_i = \{ \mathscr{Y}_{1,N_{k_{j,i}}}(k_{j,i}), \mathscr{Y}_{1,N_i}(i) \}$, where $\mathscr{Y}_{1,N_{k_{j,i}}}(k_{j,i}) = \{ \hat{\psi}_{k_{j,i}}(T_s),), \ldots, \hat{\psi}_{k_{j,i}}(N_{k_{j,i}}T_s) \}$ and $\mathscr{Y}_{1,N_i}(i) = \{ \hat{\psi}_i(T_s), \ldots, \hat{\psi}_i(N_iT_s) \}$ are two sequences of signals stored by i. Thresholds are $p_s(i)$ and $p_s(k_{j,i})$. Sample sizes are N_i and $N_{k_{j,i}}$. The Decision function is

$g: \Omega^N \rightarrow \{H_0, H_1\}$,

$$g(t_k, \mathscr{Y}_{1,N}) = \begin{cases} H_1 & \text{if } \mathscr{T}(t_k, \mathscr{Y}_i) = 1, \\ H_0 & \text{if } \mathscr{T}(t_k, \mathscr{Y}_i) = 0, \end{cases} \quad (8)$$

where Ω is the sample space, and H_0 and H_1 denote normal and faulty behaviors, respectively. $\mathscr{T}$ should thus provide the necessary knowledge on the health of the vehicle through $\hat{\psi}_{k_{j,i}}(kT_s)$ and $\hat{\psi}_i(kT_s)$. In normal operating conditions, the aforementioned sequences are correlated, whereas when a fault occurs there is an informational discrepancy between the two sequences. Comparing $\hat{\psi}_{k_{j,i}}(kT_s)$ and $\hat{\psi}_i(kT_s)$ is done with objective of reducing the level of false alarms caused by delayed transients of i following $t_1 + t_{j/k_{j,i}}$ (Fig. 5(c)) and by noisy measurements. In Fig. 5, $t_{x/y}$ denotes the propagation time of transients from x to y. Detection by i of a nonabrupt fault occurring in $j_i^F \in \mathscr{N}_i^C$ is thus carried out by analyzing and comparing the impact of faulty behavior of j_i^F on i. Such impact is detectable owing to the dynamic couplings expressed by edges of G_{FFC}. DNFD achieves fault detection by utilizing the propagation through the formation rather than directly detecting the vehicle's faulty dynamics, which may result in a slow detection process. This apparent drawback is acceptable as nonabrupt faults evolve slowly.
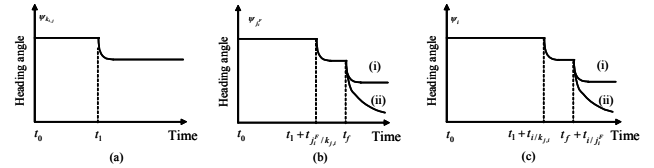
Fig. 5. Actual noise-free heading angle trajectories. (a) Vehicle $k_{j,i}$ with a change of planar orientation at t_l; (b) Vehicle j_i^F with a fault triggered at t_f. Signals emanating from j_i^F are discarded; (c) i is dynamically coupled to j_i^F.

b) Heading Angle Estimator

Each vehicle i estimates its heading angle by means of the following discrete-time, open-loop estimator

$$\begin{aligned} \gamma_{i,k+1}^f &= e^{-a_\gamma T_s} \gamma_{i,k}^f + (1 - e^{-a_\gamma T_s}) \gamma_i', \\ \phi_{i,k+1}^f &= e^{-a_\phi T_s} \phi_{i,k}^f + (1 - e^{-a_\phi T_s}) \phi_i', \\ \dot{x}_{i,k+1} &= \dot{x}_{i,k} e^{-C_x T_s/M} + \sum_j F_{ji}(1 - e^{-C_x T_s/M}) \gamma_{i,k+1}^f / C_x, \quad (9) \\ \dot{y}_{i,k+1} &= \dot{y}_{i,k} e^{-C_y T_s/M} + \sum_j F_{ji}(1 - e^{-C_y T_s/M}) \phi_{i,k+1}^f / C_y, \\ \hat{\psi}_{i,k} &= \tan^{-1}(\dot{y}_{i,k} / \dot{x}_{i,k}), \end{aligned}$$

where $1/a_\gamma$ and $1/a_\phi$ are the time constants of the filter applied to γ_i' and to ϕ_i'. Subscript k denotes the kth sample with period T_s; i.e., $\hat{\psi}_{i,k} = \hat{\psi}_i(kT_s)$. Estimator (9) results from the zero-order-hold-equivalent discretization of (1) with filtered tilt and bank angles as inputs. Closing the loop with x_i' and y_i' to robustify the estimator with respect to slowly time-varying parameters tends to deteriorate the estimate since GPS provides measurement with poor standard deviation. As the hypothesis test relies on significant changes in the heading angle (Fig. 6) steady state estimation error caused by parameter mismatch is expected not to corrupt the detection process.

c) Statistical Test for DNFD

Signal-based detectors are designed within the hypothesis testing framework [9]. This approach is generally well suited to the detection of abrupt changes and is shown to work properly when applied to (3). Since obtaining a closed-form probability distribution of $\hat{\psi}_i$ from (9) is arduous, a nonparametric detector is derived from $\hat{\psi}_i$.
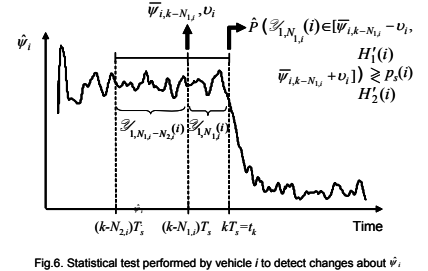
Fig.6. Statistical test performed by vehicle i to detect changes about $\hat{\psi}_i$

The decision function g in (8), implemented onboard i, is based on $\mathscr{Y}_{1,N_i}(i)$ and $\mathscr{Y}_{1,N_{k_{j,i}}}(k_{j,i})$. We present a test based on $\mathscr{Y}_{1,N_i}(i)$. The same test is applied to $\mathscr{Y}_{1,N_{k_{j,i}}}(k_{j,i})$, which enables deriving g. The vehicle i first collects $\hat{\psi}_i$ over $[(k-N_{2,i})T_s, (k-N_{1,i})T_s]$, which allows to derive empirical information utilized by the decision function (Fig. 6). Then detection that $\hat{\psi}_i$ actually changed over $[(k-N_{1,i})T_s, kT_s]$ yields a result at $kT_s = t_k$. Time average, $\overline{\psi}_{i,k-N_{1,i}}$, and bound, υ_I, are obtained empirically from sequence $\mathscr{Y}_{1,N_{1,i}-N_{2,i}}(i) = \{ \hat{\psi}_i((k-N_{2,i})T_s), \ldots,$

$\hat{\psi}_i((k-N_{1,i})T_s)\}$, as follows

$$\overline{\psi}_{i,k-N_{1,i}} = \frac{1}{N_{2,1}-N_{1,i}} \sum_{j=1}^{N_{2,1}-N_{1,i}} \psi_i((k-N_{2,i}+j)T_s),$$

$$Q\left(\mathscr{Y}_{1,N_{1,i}-N_{2,i}}(i) \in [\overline{\psi}_{i,k-N_{1,i}} - \upsilon_i, \overline{\psi}_{i,k-N_{1,i}} + \upsilon_i]\right) = \alpha, \quad (10)$$

where $\alpha \in (0,1)$ and Q denotes the empirical frequency that the elements of $\mathscr{Y}_{1,N_{1,i}-N_{2,i}}(i)$ are in the interval $[\overline{\psi}_{i,k-N_{1,i}} - \upsilon_i, \overline{\psi}_{i,k-N_{1,i}} + \upsilon_i]$. Recall that the empirical frequency $Q(\{y_1,...,y_n\} \in A)$ is defined as

$$Q(\{y_1,...,y_n\} \in A) = (1/n)\sum_{i=1}^{n} I_A(y_i), \quad (11)$$

where I stands for the indicator function. Let $p_s(i)=n_{s,i}/N_{1,i}(i)$ and $H_1'(i)$ and $H_0'(i)$ stand for time-constant and time-varying $i's$ heading angle trajectory, respectively. The statistical test to decide whether $\mathscr{Y}_{1,N_{1,i}}(i) = \{\hat{\psi}_i((k-N_{1,i})T_s), ..., \hat{\psi}_i(kT_s)\}$ is in $[\overline{\psi}_{i,k-N_{1,i}} - \upsilon_i, \overline{\psi}_{i,k-N_{1,i}} + \upsilon_i]$ with a probability of false alarms $P_F \leq p_F$ is given by

$$\hat{P}\left(\mathscr{Y}_{1,N_{1,i}}(i) \in [\overline{\psi}_{i,k-N_{1,i}} - \upsilon_i, \overline{\psi}_{i,k-N_{1,i}} + \upsilon_i]\right) \begin{array}{c} H_1'(i) \\ \gtrless \\ H_2'(i) \end{array} p_s(i) \quad (12)$$

$\hat{P}$ denotes the empirical frequency defined similarly as Q in (14) and the probability of false alarms is related to p_s as

$$\begin{aligned} P_F &= E\left[\sum_{u=1}^{N_{1,i}} I_{[\overline{\psi}_{i,k-N_{1,i}} - \upsilon_i, \overline{\psi}_{i,k-N_{1,i}} + \upsilon_i]}(\hat{\psi}_{i,(k-N_{1,i}-u+1)T_s}) > n_{s,i}\right] \\ &= \sum_{i=n_{s,i}}^{N_{1,i}} \binom{N_{1,i}}{i}\alpha^i(1-\alpha)^{N-i}. \end{aligned} \quad (13)$$

Inequality $P_F \leq p_F$ is thus obtained provided $n_{s,i}$ $(=p_s(i)N_{1,i})$ satisfies

$$\sum_{i=n_{s,i}}^{N_{1,i}} \binom{N_{1,i}}{i}\alpha^i(1-\alpha)^{N-i} \leq p_F. \quad (14)$$

The procedure (10)-(14), with $p_s(k_{j,i})=n_{s,k_{j,i}}/N_{1,k_{j,i}}(k_{j,i})$, is applied to $\mathscr{Y}_{1,N_{1,k_{j,i}}-N_{2,k_{j,i}}}(k_{j,i})$ and to $\mathscr{Y}_{1,N_{1,k_{j,i}}}(k_{j,i})$ over $[(k-N_{2,i})T_s,(k-N_{1,i})T_s]$ and $[(k-N_{1,i})T_s,kT_s]$, respectively, which leads to the selection of $H_1'(k_{j,i})$ or $H_0'(k_{j,i})$. $\mathscr{T}$, which is instrumental to the g in (11), is defined as

$$\mathscr{T}(t_k,\mathscr{Y}_i) = \begin{cases} 1 & \text{if} \begin{cases} H_0'(i)\text{ at }t=t_k \text{ and } H_1'(k_{j,i})\text{ for all }t\in[t_k-t_{dc},t_k], \\ \text{or} \\ H_1'(i)\text{ at }t=t_k \text{ and } H_0'(k_{j,i})\text{ for all }t\in[t_k-t_{dc},t_k], \end{cases} \\ 0 & \text{if} \begin{cases} H_1'(i)\text{ at }t=t_k \text{ and } H_1'(k_{j,i})\text{ for all }t\in[t_k-t_{dc},t_k], \\ \text{or} \\ H_0'(i)\text{ at }t=t_k \text{ and } H_0'(k_{j,i})\text{ for all }t\in[t_k-t_{dc},t_k]. \end{cases} \end{cases} \quad (15)$$

t_{dc} stands for the propagation time of heading angle transients between $k_{j,i}$ and i. i is dynamically coupled to $k_{j,i}$ through j_i. Thus, t_{dc} has to satisfy $t_{dc} \geq t_{i/j_i} + t_{j_i/k_{j,i}}$, where t_{i/j_i} and $t_{j_i/k_{j,i}}$ are depicted in Fig. 5. Roughly speaking, the decision function verifies whether dynamically coupled vehicles have similar behavior up to the propagation time t_{dc}, which depends on the closed-loop dynamics given in (1)-(3).

C. Decision-Making

A group of p formations, composed of n_p unmanned vehicles have to reach a set of tactical targets according to a rendezvous-type scenario. The objective consists in deriving policies (π^u, π^v) such that

$$\left(\pi_{1,P_i}^{u+}, \pi_{1,P_i}^{v+}\right) = \arg\min_{\pi_{1,P_i}^u} \max_{\pi_{1,P_i}^v} J(N_1,P_i,S_{\gamma+,1})$$

$$J(N_1,P_i,S_{\gamma+,1}) = E\left\{\sum_{\nu\in B}\left(\sum_{k=1}^{k=N-1} U_{2,k}^\nu + \sum_{k=2}^{k=N} m_p I(N_k^\nu|N_{k-1}^\nu) - S^\nu\right)\right\},$$

$$I(N_k^\nu|N_{k-1}^\nu) = \begin{cases} 1 \text{ if } N_k^\nu < N_{k-1}^\nu \\ 0 \text{ if } N_k^\nu = N_{k-1}^\nu \end{cases},$$

$$S^\nu = m_p n_p.$$

where superscripts u and v denote the policy for the formations of aerial vehicles and for the ground units, respectively. The blue team aims at maximizing the number of onboard weapons once at the tactical targets. N_k^ν represents the state of the formation ν, i.e., the number of healthy vehicles at t_k. m_p stands for the number of munitions per vehicles. The blue team is faced with ground units (red team) having the capacity to destroy the aerial vehicles. Discrete-time dynamics in N_k^ν and in the ground unit states are modeled by means of Markov decision processes that depend on u and v. Policies are obtained by solving a two-player stochastic game, where u tries to maximize the weapon effect of the blue team on the tactical target whereas v wants to protect the tactical targets by destroying as many vehicles as possible. The blue team has the capacity to subdivide into smaller formations taking multiple paths on their way to the tactical targets, so as to minimize the risk of vehicle loss. The blue team evolves in a partially known environment where the location of the ground units and their classification is not perfectly known. A one-step lookahead rollout policy is presented to derive a tractable solution to the stochastic game [5]. First, a lookup-table-based policy is obtained prior to mission by solving a dynamic programming equation that corresponds to the most dangerous ground unit and decoy configuration. However, this configuration may not represent the actual theatre for two reasons: (i) the probabilistic nature of the ground units and decoys detection and classification; (ii) the configuration of the red team may evolve. Thus, a one-step lookahead policy improvement step is implemented by using a recursive Bayesian filter that provides a distribution over the possible configurations of ground units and decoys given the last observations. Each time a vehicle is destroyed, the policy is computed from the last assessment of the state of each formation. With I-DCFD, adaptation to faulty behaviors is carried out on two fronts: (i) at the decision-making level, where the policy takes into account vehicle loss; and (ii) at the team-level dynamics where DNFD and DAFD compensate for faults/failures.

III. HIGH-FIDELITY, NONLINEAR 6-DOF SIMULATIONS

A. Case study: Integrated Decision and Control

The proposed I-DCFD is demonstrated, by means of high-fidelity models of a multiformation fleet of nine nonlinear 6-DOF airships. Each formation is allowed to be composed of three or more vehicles, and to exchange relevant information via the network, which is subject to failure. The reader is

referred to [4] for details on vehicle dynamics. Sensor noise and actuator nonlinearities are part of the models. The four types of actuator faults are modeled according to (3) and Fig. 3. For the modeling and simulation of body damage, we assume that a projectile blast occurring near an airship results in a sudden loss of buoyancy. Simulations are carried out for a base-to-target rendezvous mission assuming perfect information on the adversary. The probabilities used in the simulations are given in [5]. When a formation is hit by enemy fire, the blue team vehicle experiencing body damage is determined randomly. Body damage may occur concurrently with network faults. Paths and PH trajectories obtained with the simulations are shown in Fig. 7. At t=0 s, 3-vehicle formations {1,2,3} take off and reach, after a short transient, elevations of 5 m, 7 m, and 9 m, respectively. The particular realization of the MPDs used in the simulations entails a loss of three vehicles during mission. Such losses are caused by body damage. At the low-level control, I-DCFD allows detecting the loss of a vehicle by using proximity sensors, such as video or sonar, and then adapting, both the trajectory generation and the formation control, by following the nearest non-faulty neighboring vehicle that is located ahead in the formation, according to the information flow. At the higher level of the hierarchy, the decision making adapts to the loss of the vehicles by deriving policy (19).

(a) (b)
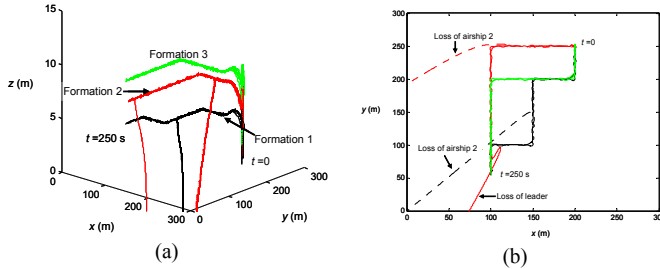
Fig. 7: (a) 3D trajectories and (b) 2D trajectories obtained with I-DCFD.
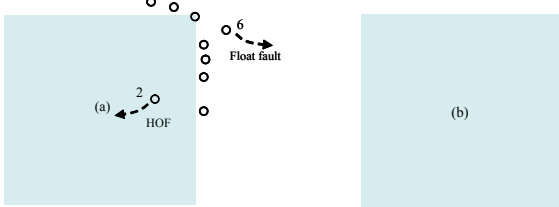
Fig. 8. (a) Simultaneous fault occurrence and loss of vehicles 2 and 6. (b) Formation stabilization with larger intervehicle distances.

B. Case study: Concurrent Nonabrupt and Abrupt Faults

For a string of nine vehicles {1,…,9}, two simultaneous faults are triggered at $t=t_f$. Vehicle 2 experiences a HOF on one of its actuators, whereas vehicle 6 is subject to a float-type fault. These faults are detected by means of DAFD and DNFD implemented onboard vehicles 3 and 7, respectively. Based on (5), the HOF in one actuator of vehicle 2 is

$$\delta_i = 1_{t-t_f}(H_{OF,t-t_f}(F_{in}(t)) - F_{in}(t))$$

$$H_{OF,t-t_f}(x) = \begin{cases} x, & \text{if } t - t_f < 0, \\ 3.5\,\text{N}, & \text{otherwise,} \end{cases} \qquad (17)$$

where 1_{t-t_f} is the Heaviside function. The leader of the formation is required to follow a square-like PH curve, despite the faults. Snapshots of the formation time trajectories are depicted in Fig. 8 to obtain a better insight of formation cohesiveness. Integrity of the formation is preserved since the abnormal behavior is detected sufficiently fast and corrective actions are taken.

IV. Conclusions

This paper proposed a hierarchical and decentralized scheme for integrated decision, control and fault detection in cooperating unmanned aerial systems flying in formations. The decision-control system builds upon a formation controller and a trajectory generator, abrupt and nonabrupt fault detectors, and a tractable decision policy. High-fidelity 6-DOF simulations carried out for a rendezvous mission showed that concurrent faults can be detected and effectively compensated for both at the formation control and at the decision-making levels.

References

[1] M. Valenti, B. Bethke, J.P. How, D.P. de Farias, and J.L. Vian, "Embedding Health Management into Mission Tasking for UAV Teams", *Proceedings of American Control Conference 2007*, NY.

[2] M. Innocenti and L. Pollini, "Management of Communication Failures in Formation Flight," *Journal of Aerospace Computing, Information, and Communication*, Vol. 1, pp. 19-35, January 2004.

[3] R.K. Mehra, J.D. Boskovic and S.-M Li, "Autonomous formation flying of multiple UCAVs under communication failure," *IEEE Position Location and Navigation Symposium*, pp. 371—378, 2000.

[4] N. Léchevin and C.A. Rabbath, "Robust Decentralized Fault Detection in Leader-to-Follower Formations of Uncertain, Linearly Parameterized Systems", *Journal of Guidance, Control and Dynamics,* Vol. 30, No.5, September-October 2007, 1528-1535.

[5] N. Léchevin, C.A. Rabbath, and M. Lauzon, "A Decision Policy for the Routing and Munitions Management of Multiformations of Unmanned Combat Vehicles in Adversarial Urban Environments," *IEEE Trans. on Control Systems Technology*, under press, 2007.

[6] N. Léchevin, C.A. Rabbath, and P. Sicard, "Trajectory Tracking of Leader-Follower Formations Characterized by Constant Line-of-Sight Angles," *Automatica*, Vol. 42, pp. 2131-2141, December 2006.

[7] J.D. Boskovic, S.E. Bergstrom, and R.K. Mehra, "Robust Integrated Control Design Under Failures, Damage, and State-Dependant Disturbances," *Journal of Guidance, Control, and Dynamics,* Vol. 28, No. 5, pp. 902-917, 2005.

[8] D. Shore and M. Bodson, "Flight Testing of a Reconfigurable Control System on an Unmanned Aircraft," *Journal of Guidance, Control, and Dynamics,* Vol. 28, No. 4, pp. 698-707, 2005.

[9] M. Basseville and I.V. Nikiforov, *Detection of Abrupt Changes*, Prentice-Hall, Englewoods Cliffs, N.J., April 1993.

[10] Madhavan Shanmugavel, Antonios Tsourdos, Brian A White and Rafał Żbikowski, "Differential geometric path planning of Multiple UAVs", *ASME Journal of Dynamic Systems, Measurement and Control*, Sept. 2007, Vol 129, Issue 5, pp.620-632.